Nonlinear Response and Stability Analysis of Beams Using Finite Elements in Time

O. A. Bauchau* and C. H. Hong†
Rensselaer Polytechnic Institute, Troy, New York

The dynamic response and stability analysis of beams undergoing large deflections and rotations is analyzed using the finite-element method in time. This formulation provides an efficient and consistent approach to predicting the dynamic response of nonlinear periodic systems as well as their stability boundaries based on Floquet's theory. This paper has two goals: 1) to present the formulation of the finite element in time equations for naturally curved and twisted beams undergoing large deflections and rotations, and 2) to discuss the predictions of this method when applied to several classical nonlinear beam problems for which analytical solutions exist and, in some cases, experimental results are available. These examples are 1) the natural vibration frequencies of a rotating beam, 2) the harmonic and superharmonic response of a clamped-clamped beam undergoing large-amplitude vibrations, 3) the dynamic instability of a cantilevered beam under a tip follower force, and 4) the parametric excitation of a beam under an axial pulsating load, with and without the presence of viscous damping forces. In all cases, close agreement is found between the analytical results and the predictions of the finite element in time approach, which appears to be an efficient and reliable technique for nonlinear dynamic response and stability analysis of periodic systems.

I. Introduction

WHEN confronted with a dynamic problem, the structural analyst generally proceeds in two steps. First, the structure is discretized spatially using the finite-element method or a modal superposition approach, for instance, hence reducing the problem to a set of differential equations in time that can then be solved with the help of a variety of time-stepping procedures.[1-3] Another possible approach is the use of the finite element in time (FET) method based on Hamilton's classical principle.[4-6] This approach has not gained much popularity because it results in very large systems of equations (all the spatial degrees of freedom at all time steps are coupled together) that must be solved iteratively when dealing with a nonlinear dynamic problem. Furthermore, if the shape functions are selected as a product of space- and time-varying functions, the resulting equations can be cast in a form identical to that of time-stepping methods.

There are, however, two specific advantages to the finite element in time formulation. First, nonlinear systems with periodic boundary conditions can be readily analyzed, in contrast with time-stepping methods, which require initial conditions to start up the time integration procedure so that periodic boundary conditions cannot be readily imposed. Periodic boundary conditions present no specific difficulty for the FET method: initial and final displacements and velocities can be readily made identical when assembling the global finite-element equations. In addition, stability analysis of the nonlinear periodic solution is often important, and Floquet's theory[10] can be used for this task, requiring the evaluation of the transition matrix of the system, which happens to be a by-product of the FET procedure.

The second advantage is the straightforward derivation of higher-order approximations in time, which are unconditionally stable when reduced integration in time is used. Furthermore, as discussed in Ref. 6, the second-order FET approximation yields an accuracy superior to that of more conventional schemes such as the Houbolt,[1] Newmark,[2] or Wilson et al.[3] methods at identical computational cost. Although other unconditionally stable, higher-order integration schemes are available,[7-9] the FET formulation allows a particularly simple derivation. Higher-order FET approximations are simply obtained by changing the degree of the interpolation functions in time.

The focus of this paper is the periodic dynamic response and stability analysis of naturally curved and twisted beams undergoing large displacements and rotations. The strain energy expression of this problem was obtained in Refs. 11 and 12, and the kinetic energy expression as well as the FET equations will be derived in the present paper. The accuracy and reliability of this formulation will be assessed by analyzing a number of classical nonlinear periodic beam problems and comparing the FET predictions to existing analytical solutions as well as experimental results when available.

The first problem is the calculation of the natural vibration frequencies of a rotating cantilevered beam (the natural frequencies are obtained as the eigenvalues of the transition matrix, calculated by FET). Then, the harmonic and superharmonic response of a clamped-clamped beam undergoing large-amplitude vibrations will be investigated. Next, the analysis of a cantilevered beam under a tip follower force will demonstrate the stability boundary prediction capabilities of the method. Finally, the parametric excitation of a beam under an axial pulsating load is investigated with and without the presence of viscous damping forces. In all cases, close agreement is found between the analytical results and the predictions of the FET approach.

II. Strain Energy Expression

Consider the naturally curved and twisted beam depicted in Fig. 1. The triad i_1, i_2, i_3 is fixed in space, and the triad e_1, e_2, e_3 is attached at a reference line along the axis of the beam. The tangent to the reference line is e_1, and e_2 and e_3 define the

Received Aug. 6, 1987; revision received Feb. 16, 1988.

*Assistant Professor, Department of Mechanical Engineering, Aeronautical Engineering and Mechanics. Member AIAA.

†Graduate Assistant, Department of Mechanical Engineering, Aeronautical Engineering and Mechanics. Member AIAA.

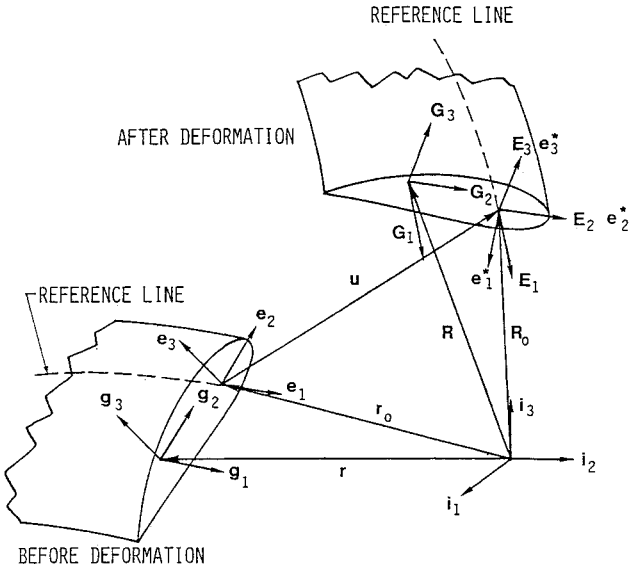

Fig. 1 Geometry of the beam before and after deformation.

plane of the cross section. The curvilinear coordinates along this triad are x_1, x_2, and x_3, respectively. The position vector of a material particle of the beam is

$$\boldsymbol{r}=\boldsymbol{r}(x_1,x_2,x_3) \tag{1}$$

After deformation, the same particle has a position vector:

$$\boldsymbol{R}=\boldsymbol{R}(x_1,x_2,x_3) \tag{2}$$

The corresponding vectors at the reference line are

$$\boldsymbol{r}_0=\boldsymbol{r}_0(x_1,0,0) \tag{3a}$$

$$\boldsymbol{R}_0=\boldsymbol{R}_0(x_1,0,0) \tag{3b}$$

and the displacement vector of the reference line is given by

$$\boldsymbol{u}=\boldsymbol{R}_0-\boldsymbol{r}_0 \tag{4}$$

At the reference line, the base vector[13,14] in the deformed and undeformed positions, respectively, are

$$\boldsymbol{e}_i=\boldsymbol{r}_{,i}\,|_{x_2=x_3=0} \tag{5a}$$

$$\boldsymbol{E}_i=\boldsymbol{R}_{,i}\,|_{x_2=x_3=0} \tag{5b}$$

The fundamental assumption of beam theory is that the cross section does not deform in its own plane. Hence, the base vectors $\boldsymbol{E}_2$ and $\boldsymbol{E}_3$, which are in the plane of the cross section after deformation, are mutually orthogonal unit vectors, since they correspond to a translation and rotation of the base vectors $\boldsymbol{e}_2$ and $\boldsymbol{e}_3$ of the original configuration. In contrast, $\boldsymbol{E}_1$ is no longer unit or orthogonal to $\boldsymbol{E}_2$ or $\boldsymbol{E}_3$, as axial and shearing strains are allowed.

The triad $\boldsymbol{e}_i^*$ is defined as follows:

$$\boldsymbol{e}_2^*=\boldsymbol{E}_2,\quad \boldsymbol{e}_3^*=\boldsymbol{E}_3 \tag{6a}$$

$$\boldsymbol{e}_1^*=\boldsymbol{e}_2^*\times\boldsymbol{e}_3^* \tag{6b}$$

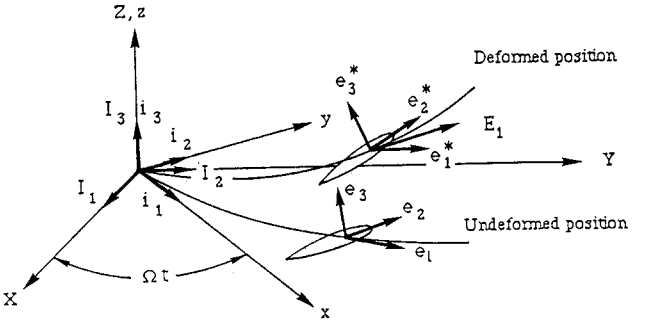

Fig. 2 Axes systems of the rotating beam.

This triad can be related to the basic reference triad through an unknown rotation matrix $T(x_1)$:

$$\begin{bmatrix} \boldsymbol{e}_1^* \\ \boldsymbol{e}_2^* \\ \boldsymbol{e}_3^* \end{bmatrix} = T^T(x_1) \begin{bmatrix} \boldsymbol{i}_1 \\ \boldsymbol{i}_2 \\ \boldsymbol{i}_3 \end{bmatrix} \tag{7}$$

In Ref. 11, the strain energy U stored in the beam was obtained in the following form:

$$U=\frac{1}{2}\int_0^L \boldsymbol{e}^T\boldsymbol{H}\boldsymbol{e}\,\mathrm{d}x_1 \tag{8}$$

Where L is the span of the beam, H the stiffness matrix, and $\boldsymbol{e}^T$ the vector of strain components that nonlinearly depends on the kinematic variables of the problem:

$$\boldsymbol{e}^T=\boldsymbol{e}^T(u_1,u_1',u_2,u_2',u_3,u_3',\alpha,\alpha',\beta,\beta',\gamma,\gamma',\delta,\delta')=\boldsymbol{e}^T(q^T) \tag{9}$$

where u_i are the components of the displacement vector in the i_1 triad, α, β, γ the orientation angles used to represent the rotation matrix T, δ the magnitude of the torsional warping deformation, and $(\,)'$ denotes derivative with respect to x_1. The sequence of the orientation angle was selected to avoid the singularities at zero rotation.[12] The explicit form of the strain components and stiffness matrix are given in Ref. 11.

III. Kinetic Energy Expression

We now turn our attention to the kinetic energy of the system. We assume that the beam is rotating at a constant angular velocity Ω about the axis I_3 of an inertial reference frame I_i (see Fig. 2). The time derivative of the triad i_1 is

$$\begin{bmatrix} \dot{i}_1 \\ \dot{i}_2 \\ \dot{i}_3 \end{bmatrix} = \begin{bmatrix} 0 & \Omega & 0 \\ -\Omega & 0 & 0 \\ 0 & 0 & 0 \end{bmatrix} \begin{bmatrix} i_1 \\ i_2 \\ i_3 \end{bmatrix} = \omega_g \begin{bmatrix} i_1 \\ i_2 \\ i_3 \end{bmatrix} \tag{10}$$

where $(\,)^{\cdot}$ is used to denote time derivative.

Since the cross section does not deform in its own plane, the position vector of a material particle in the deformed configuration can be written as

$$\boldsymbol{R}=\boldsymbol{R}_0+x_2\boldsymbol{E}_2+x_3\boldsymbol{E}_3=\boldsymbol{r}_0+\boldsymbol{u}+x_2\boldsymbol{e}_2^*+x_3\boldsymbol{e}_3^* \tag{11}$$

In the derivation of the strain energy expression, axial displacement components were added to represent the warping deformations [see Ref. 11, Eq. (15)]. However, we assume here that the inertia force associated with the warping

displacements are very small and hence can be neglected. Expressing $\boldsymbol{R}$ in the i_1 triad and using Eq. (7), we obtain

$$\boldsymbol{R} = \lfloor i_1, i_2, i_3 \rfloor \left\{ \begin{bmatrix} x_0 + u_1 \\ y_0 + u_2 \\ z_0 + u_3 \end{bmatrix} + T \begin{bmatrix} 0 \\ x_2 \\ x_3 \end{bmatrix} \right\} \tag{12}$$

where x_0, y_0, z_0 are the components of the vector $\boldsymbol{r}_0$ in the i_i triad. The inertial time derivative of the position vector is readily obtained by combining Eqs. (10) and (12):

$$\boldsymbol{R}^{\cdot} = \lfloor i_1, i_2, i_3 \rfloor \left\{ \begin{bmatrix} \dot{u}_1 \\ \dot{u}_2 \\ \dot{u}_3 \end{bmatrix} + \omega^T T \begin{bmatrix} 0 \\ x_2 \\ x_3 \end{bmatrix} \right\} \tag{13}$$

where the total rotation matrix $\omega^T = \omega_l^T + \omega_g^T$, the local rotation matrix $\omega_l^T = T^{\cdot} T^T$, and

$$\tilde{u}^{\cdot} = \begin{bmatrix} \dot{u}_1 \\ \dot{u}_2 \\ \dot{u}_3 \end{bmatrix} = \begin{bmatrix} u_1^{\cdot} - \Omega(y_0 + u_2) \\ u_2^{\cdot} + \Omega(x_0 + u_1) \\ u_3^{\cdot} \end{bmatrix} \tag{14}$$

The kinetic energy T of the beam is

$$T = \frac{1}{2} \int_0^L \int_\Gamma \rho \boldsymbol{R}^{\cdot} \cdot \boldsymbol{R}^{\cdot} \, ds \, dx_1 \tag{15}$$

where s is the curvilinear variable that describes the thin-walled contour Γ of the cross section, and ρ is the density of the material. Combining Eqs. (13) and (15), the kinetic energy becomes

$$T = \frac{1}{2} \int_0^L v^T I v \, dx_1 \tag{16}$$

where I is the mass matrix whose terms are defined in Appendix A, and

$$v^T = \lfloor \bar{u}_1^{*\cdot}, \bar{u}_2^{*\cdot}, \bar{u}_3^{*\cdot}, \omega_1^*, \omega_2^*, \omega_3^* \rfloor \tag{17}$$

The first three terms of this vector represent the velocity components in the $\boldsymbol{e}_i^*$ triad $\tilde{u}^{*\cdot} = T^T \tilde{u}^{\cdot}$, and the last three terms represent the total angular velocities in the $\boldsymbol{e}_i^*$ triad given by

$$\begin{bmatrix} \omega_1^* \\ \omega_2^* \\ \omega_3^* \end{bmatrix} = \begin{bmatrix} -S\beta & 0 & 1 \\ -C\beta C\gamma & S\gamma & 0 \\ C\beta S\gamma & C\gamma & 0 \end{bmatrix} \begin{bmatrix} \alpha^{\cdot} \\ \beta^{\cdot} \\ \gamma^{\cdot} \end{bmatrix} + \Omega \begin{bmatrix} T_{31} \\ T_{32} \\ T_{33} \end{bmatrix} \tag{18}$$

where $S\beta = \sin\beta$, $C\gamma = \cos\gamma$, etc., and T_{ij} are the components of the matrix T. The velocity vector v^T is a function of the kinematic variables and their time derivatives:

$$v^T = v^T(u_1^{\cdot}, u_2^{\cdot}, u_3^{\cdot}, \alpha^{\cdot}, \beta^{\cdot}, \gamma^{\cdot}, u_1, u_2, u_3, \alpha, \beta, \gamma) = v^T(\tilde{q}^T) \tag{19}$$

IV. Lagrangian Expression

The Lagrangian of a mechanical system is defined as $\mathcal{L} = T - U$ and can be readily obtained by subtracting Eq. (8) from Eq. (16). However, this expression is strongly nonlinear, since it depends on powers of the displacement functions and products of trigonometric functions of the orientation angles. In order to obtain a form suitable for finite-element modeling, the Lagrangian expression will be expanded about a known reference configuration using a quasilinearization technique:[15]

$$\mathcal{L} = \int_0^L \left(\bar{T} + \boldsymbol{L}^T \Delta\tilde{q} + \frac{1}{2} \Delta\tilde{q}^T N \Delta\tilde{q} - \bar{U} - \boldsymbol{G}^T \Delta q - \frac{1}{2} \Delta q^T J \Delta q \right) dz \tag{20}$$

where $\bar{(\,)}$ denotes a quantity evaluated in the reference configuration, Δ denotes a small change in the corresponding quantity, $\boldsymbol{L}^T$ and $\boldsymbol{G}^T$ are the equivalent load vectors for inertia and elastic forces, respectively,

$$\boldsymbol{L}^T = \frac{\partial T}{\partial \tilde{q}} \tag{21a}$$

$$\boldsymbol{G}^T = \frac{\partial U}{\partial q} \tag{21b}$$

and the components of the mass and stiffness matrix, respectively, are

$$N_{ij} = \frac{\partial^2 T}{\partial \tilde{q}_i \partial \tilde{q}_j} \tag{22a}$$

$$J_{ij} = \frac{\partial^2 U}{\partial q_i \partial q_j} \tag{22b}$$

It is now possible to apply standard finite-element techniques to spatially discretize the displacement and rotation functions. In this effort, all functions were interpolated using standard cubic shape functions:

$$q = B\hat{u} \tag{23}$$

$$\tilde{q} = \begin{bmatrix} \tilde{B} & 0 \\ 0 & \tilde{B} \end{bmatrix} \begin{bmatrix} \hat{u}^{\cdot} \\ \hat{u} \end{bmatrix} \tag{24}$$

where B and $\tilde{B}$ are the shape function matrices,[16] and $\hat{u}$ is the vector of nodal displacements. The Lagrangian now can be calculated by introducing Eqs. (23) and (24) into Eq. (20), then integrating over the span of the beam to yield

$$\mathcal{L} = \lfloor \Delta\hat{u}^{T\cdot}, \Delta\hat{u}^T \rfloor \left\{ \begin{bmatrix} S \\ \bar{S} - F \end{bmatrix} + \frac{1}{2} \begin{bmatrix} M & \tilde{M} \\ \tilde{M}^T & \tilde{M} - K \end{bmatrix} \begin{bmatrix} \Delta\hat{u}^{\cdot} \\ \Delta\hat{u} \end{bmatrix} \right\} \tag{25}$$

where the equivalent load vector (for elastic forces) and stiffness matrix are, respectively,

$$F = \int_0^L B^T G \, dx_1 \tag{26a}$$

$$K = \int_0^L B^T J B \, dx_1 \tag{26b}$$

and the equivalent load vector (for inertia forces) and the mass matrix are, respectively,

$$\begin{bmatrix} S \\ \bar{S} \end{bmatrix} = \int_0^L \begin{bmatrix} \tilde{B}^T & 0 \\ 0 & \tilde{B}^T \end{bmatrix} \boldsymbol{L} \, dx_1 \tag{27a}$$

$$\begin{bmatrix} M & \tilde{M} \\ \tilde{M}^T & \tilde{M} \end{bmatrix} = \int_0^L \begin{bmatrix} \tilde{B}^T & 0 \\ 0 & \tilde{B}^T \end{bmatrix} N \begin{bmatrix} \tilde{B} & 0 \\ 0 & \tilde{B} \end{bmatrix} dx_1 \tag{27b}$$

V. Work Done by the Applied Loads

In this effort, three types of loads were considered: the known, conservative forces ("dead loads"), axial follower forces (the force of constant magnitude acting along the deformed axis of the beam e_1^*), and viscous-type damping forces. These forces may vary continuously along the axis of the beam, and nodal values can be obtained using the usual energy considerations.[16] The virtual work done by the forces applied at one specific node can be written as

$$\delta W_n = \delta \hat{\boldsymbol{u}}_n^T \boldsymbol{Q}_n \tag{28}$$

where $\delta \hat{\boldsymbol{u}}_n^T$ is the virtual nodal displacement vector at one node and $\boldsymbol{Q}_n$ the nodal load vector at one node that can be expressed as

$$\boldsymbol{Q}_n = \begin{bmatrix} F_1 - F_f T_{11} - \mu_1 u_1^{\cdot} \\ F_2 - F_f T_{21} - \mu_2 u_2^{\cdot} \\ F_3 - F_f T_{31} - \mu_3 u_3^{\cdot} \\ F_\alpha \quad -\mu_\alpha \alpha^{\cdot} \\ F_\beta \quad -\mu_\beta \beta^{\cdot} \\ F_\gamma \quad -\mu_\gamma \gamma^{\cdot} \end{bmatrix} \tag{29}$$

where F_i are the nodal components of the dead loads and moments, F_f the magnitude of the follower force, T_{ij} the components of the rotation matrix T of Eq. (7), and μ_i the viscous damping constants. Once again, this expression contains nonlinear terms due to the nonconservative forces; hence, quasilinearization was used once again about a known reference configuration to expand the load vector as

$$\boldsymbol{Q}_n = \tilde{\boldsymbol{Q}}_n + \tilde{D}_n \Delta \hat{\boldsymbol{u}}_n^{\cdot} + D_n \Delta \hat{\boldsymbol{u}}_n \tag{30}$$

The matrices $\tilde{D}_n$ *and* D_n are defined in Appendix B. Finally, a similar expression can be written at each node, and the global nodal load vector becomes

$$\begin{bmatrix} 0 \\ \boldsymbol{Q} \end{bmatrix} = \begin{bmatrix} 0 \\ \tilde{\boldsymbol{Q}} \end{bmatrix} + \begin{bmatrix} 0 & 0 \\ \tilde{D} & D \end{bmatrix} \begin{bmatrix} \Delta \hat{\boldsymbol{u}}^{\cdot} \\ \Delta \hat{\boldsymbol{u}} \end{bmatrix} \tag{31}$$

The total virtual work of the system becomes

$$\delta W = \lfloor \delta \hat{\boldsymbol{u}}^{\cdot}, \delta \hat{\boldsymbol{u}} \rfloor \begin{bmatrix} 0 \\ \boldsymbol{Q} \end{bmatrix} \tag{32}$$

VI. Hamilton's Principle

For a mechanical system defined by the nodal displacement vector $\hat{\boldsymbol{u}}$, Hamilton's Weak Principle[4-6] writes

$$\int_{t_i}^{t_f} (\delta \mathfrak{L} + \delta W) \mathrm{d}t = \delta \hat{\boldsymbol{u}}^T \cdot \hat{\boldsymbol{p}} \Big|_{t_i}^{t_f} \tag{33}$$

where t_i, t_f is the time interval to be analyzed, and $\hat{\boldsymbol{p}}$ is the vector of generalized nodal momentums. Introducing Eqs. (25) and (32) into Eq. (33) yields

$$\int_{t_i}^{t_f} \lfloor \delta \hat{\boldsymbol{u}}^{T\cdot}, \delta \hat{\boldsymbol{u}}^T \rfloor \cdot \left\{ \begin{bmatrix} S \\ \tilde{S} - F + Q \end{bmatrix} + \begin{bmatrix} M & \tilde{M} \\ \tilde{M}^T + \tilde{D} & \tilde{M} + D - K \end{bmatrix} \begin{bmatrix} \Delta \hat{\boldsymbol{u}}^{\cdot} \\ \Delta \hat{\boldsymbol{u}} \end{bmatrix} \right\} \mathrm{d}t = \delta \hat{\boldsymbol{u}}^T \cdot \hat{\boldsymbol{p}} \Big|_{t_i}^{t_f} \tag{34}$$

The time-dependent nodal displacement vector is now discretized with standard shape functions:[16]

$$\begin{bmatrix} \hat{\boldsymbol{u}}^{\cdot} \\ \hat{\boldsymbol{u}} \end{bmatrix} = G \tilde{\boldsymbol{u}} \tag{35}$$

where G is the matrix of shape functions and $\tilde{\boldsymbol{u}}$ the vector of nodal displacements at the various time points,

$$\tilde{\boldsymbol{u}}^T = \lfloor \hat{\boldsymbol{u}}_1^T, \hat{\boldsymbol{u}}_2^T, \hat{\boldsymbol{u}}_3^T, \ldots, \hat{\boldsymbol{u}}_{N-1}^T, \hat{\boldsymbol{u}}_N^T \rfloor \tag{36}$$

$\hat{\boldsymbol{u}}_i$ are the nodal displacement values at the ith time station, and N is the total number of time stations used in the discretization. In this effort, quadratic, cubic, and quartic interpolation functions were used. Introducing Eq. (35) into (34), integrating over time, and using the extremum property of Hamilton's principle results in

$$\boldsymbol{K} \Delta U = \boldsymbol{P} - \boldsymbol{F} \tag{37}$$

where $\boldsymbol{P}$ is the global vector of generalized momenta

$$\boldsymbol{P}^T = \lfloor -\hat{\boldsymbol{p}}_1, 0, 0, \ldots, 0, \hat{\boldsymbol{p}}_N \rfloor \tag{38}$$

where $\boldsymbol{F}$ the global vector of equivalent loads

$$\boldsymbol{F} = \int_{t_i}^{t_f} G^T \begin{bmatrix} S \\ \tilde{S} - F + Q \end{bmatrix} \mathrm{d}t \tag{39}$$

and $\boldsymbol{K}$ the stiffness matrix of the entire time dependent system

$$\boldsymbol{K} = \int_{t_i}^{t_f} G^T \begin{bmatrix} M & \tilde{M} \\ \tilde{M}^T + \tilde{D} & M + D - K \end{bmatrix} G \, \mathrm{d}t \tag{40}$$

The linear system of Eq. (37) can be solved iteratively to find the time response of nonlinear dynamic systems. When the norm of the right-hand-side vector becomes small, convergence is attained. Note that the system stiffness matrix $\boldsymbol{K}$ is not symmetric due to the presence of the nonconservative loads that are responsible for the unsymmetric matrices $\tilde{D}$ and D. If the system is periodic, the momenta vector vanishes, since the periodic boundary condition requires both displacements and velocities to be identical at t_i and t_f, i.e., $\hat{u}_1 = \hat{u}_N$ and $\hat{p}_1 = \hat{p}_N$.

Such conditions are readily imposed when assembling the global FET equations. Once the periodic solution is found, a linearized stability analysis can be performed by considering small perturbation of the boundary conditions. All the intermediate time nodes can be eliminated; hence, Eq. (37) reduces to

$$\begin{bmatrix} \boldsymbol{K}_{ii} & \boldsymbol{K}_{if} \\ \boldsymbol{K}_{fi} & \boldsymbol{K}_{ff} \end{bmatrix} \begin{bmatrix} \Delta \hat{\boldsymbol{u}}_i \\ \Delta \hat{\boldsymbol{u}}_f \end{bmatrix} = \begin{bmatrix} -\Delta \hat{\boldsymbol{p}}_i \\ \Delta \hat{\boldsymbol{p}}_f \end{bmatrix} \tag{41}$$

Finally, the transition matrix of the system is found by rearranging Eq. (41) to relate initial and final perturbations:

$$\begin{bmatrix} -\boldsymbol{K}_{ff}\boldsymbol{K}_{if}^{-1} & \boldsymbol{K}_{fi} - \boldsymbol{K}_{ff}\boldsymbol{K}_{if}^{-1}\boldsymbol{K}_{ii} \\ -\boldsymbol{K}_{if}^{-1} & -\boldsymbol{K}_{if}^{-1}\boldsymbol{K}_{ii} \end{bmatrix} \begin{bmatrix} \Delta \hat{\boldsymbol{p}}_i \\ \Delta \hat{\boldsymbol{u}}_i \end{bmatrix} = \begin{bmatrix} \Delta \hat{\boldsymbol{p}}_f \\ \Delta \hat{\boldsymbol{u}}_f \end{bmatrix} \tag{42}$$

Acording to Floquet's theory,[10] the stability of the system can be assessed by calculating the eigenvalues of this transition matrix. It is interesting to note that the solution of Eq. (37) can be obtained without actually assembling the global stiffness matrix $\boldsymbol{K}$; when a new time element is generated, the internal time nodes can be eliminated, keeping as only unknown $\hat{\boldsymbol{u}}_i$ and $\hat{\boldsymbol{u}}_k$, the nodal values at the end of the current time step. Hence, the same solution algorithm can be used for both the periodic response and stability calculations.

Table 1 Normalized vibration frequencies of a rotating beam

	First flap		Second flap		First lead-lag	
λ	Ref. 14	FET	Ref. 14	FET	Ref. 14	FET
0	3.516	3.519	22.03	22.06	3.516	3.519
2	4.137	4.137	22.61	22.81	3.622	3.624
4	5.585	5.585	24.27	24.35	3.898	3.905
6	7.360	7.376	26.81	26.98	4.263	4.288
8	9.257	9.290	30.00	30.27	4.657	4.718
10	11.21	11.26	33.64	33.98	5.049	5.166
12	13.18	13.26	37.60	38.03	5.427	5.617

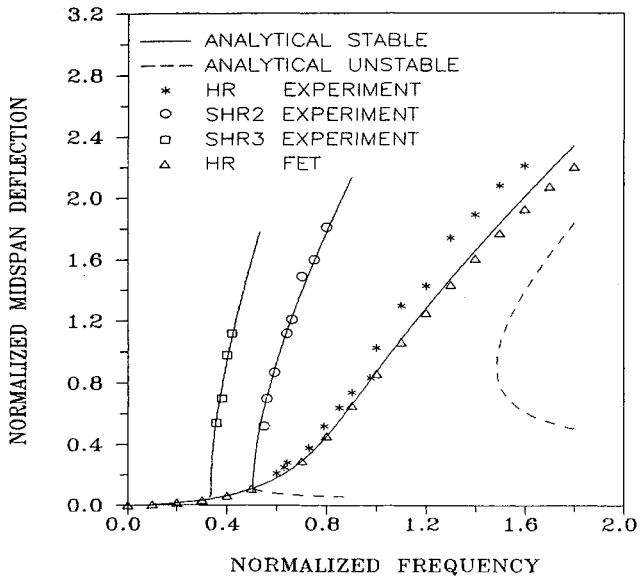

Fig. 3 Harmonic and superharmonic response of a clamped-clamped beam.

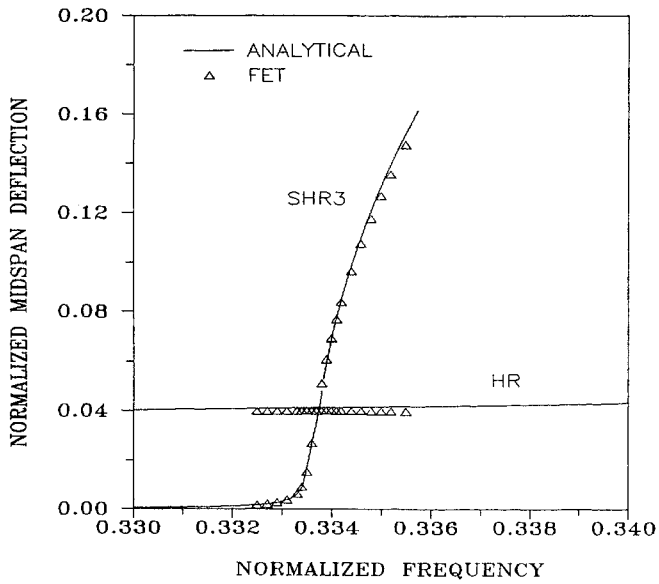

Fig. 4 Detail of the superharmonic response SHR3.

In Eqs. (39) and (40), the time integration was performed numerically using Gaussian integration. For periodic response calculation, the number of Gauss points was chosen equal to the degree of the interpolation shape function plus one to provide best accuracy, whereas for stability calculations, reduced integration was employed, as this provides unconditionally stable time-integration algorithms.[6]

VII. Numerical Examples

The first example deals with the identification of the natural vibration frequencies of a cantilevered beam of length $L=0.508$ m, rotating at an angular velocity Ω. The properties of the beam are as follows: flap bending stiffness (out of the plane of rotation) $EI_f=2.446$ Nm^2, lead-lag bending stiffness (in the plane of rotation) $EI_l=36.27$ Nm^2, and mass per unit span $m=0.113$ kg/m. Two cubic elements were used along the span of the beam, and 32 times nodes (four quartic time elements) were used to model one period. The natural frequencies and mode shapes were obtained from the eigenvalues and eigenvectors of the transfer matrix. Table 1 lists the normalized natural frequencies μ and the normalized angular velocities λ, defined as

$$\mu=\omega(mL^4/EI)^{1/2} \tag{43a}$$

$$\lambda=\Omega(mL^4/EI)^{1/2} \tag{43b}$$

for the FET approximation and a reference solution obtained by Hodges and Rutkowski.[17] Good correlation is found for both flap and lead-lag frequencies at the various angular velocities.

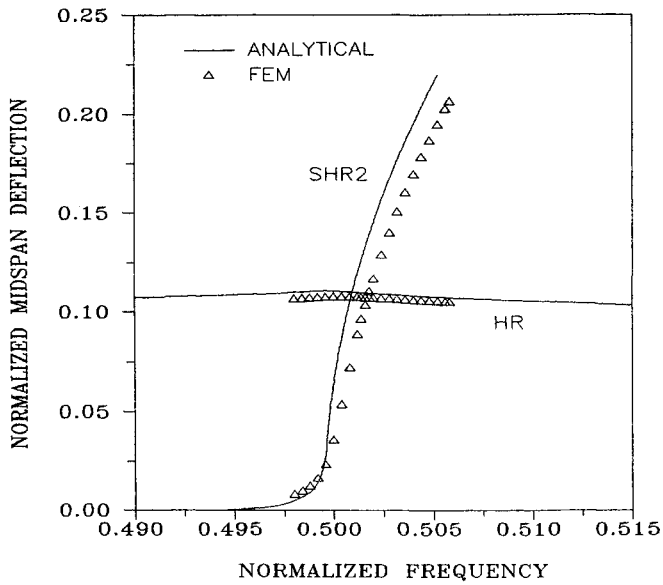

Fig. 5 Detail of the superharmonic response SHR2 (the FET results were obtained for a beam with an initial imperfection).

In the second example, the harmonic response (HR) and superharmonic response (SHR) of a clamped-clamped beam were analyzed. The properties of the beam are as follows: $L=0.457$ m, $EI=3.21\times10^{-2}$ Nm^2, and $m=5.19\times10^{-2}$ kg/m. An initial extensional strain of 5.76 μm/m was present. Two cubic elements were used to model the beam with four quartic elements in time.

Tseng and Dugundji[18] analyzed this problem using the harmonic balance (HB) method and also reported experimental results obtained from a shake test. Figure 3 compares the experimental results and analytical solutions of Ref. 18 with the present FET solutions. The normalized midspan deflection $\bar{w}$ is plotted vs the normalized excitation frequency $\bar{\omega}$, defined as

$$\bar{w} = (w/h) \cdot (1/\bar{\omega}) \tag{44a}$$

$$\bar{\omega} = \omega_f/\omega_1 \tag{44b}$$

where w is the midspan deflection, h the height of the beam, ω_1 the first natural bending frequency of the undeformed beam, and ω_f the excitation frequency. The analytical predictions of the harmonic solution are found in good agreement with the FET solution. Both solutions agree closely with the experimental results, except for large amplitude, where theory slightly underpredicts midspan displacements.

Superharmonic response can occur around integer values of the normalized excitation frequency $\bar{\omega}$. We will concentrate here on the superharmonic responses of order 2 and 3 (SHR2 and SHR3, respectively). Figure 4 shows the detailed response around $\bar{\omega} \cong 1/3$, i.e., SHR3. The response consists of the superposition of vibration at frequencies ω_f and $3\omega_f$; in other words, the beam responds at the excitation frequency but also at its own natural frequency $\omega_1 \cong 3\omega_f$. To capture the SHR3, it is necessary to increase the number of time nodes to 32 (eight quartic elements). The FET response was analyzed using the fast Fourier transform to obtain the amplitudes of the various harmonics.

Next, the SHR2 was investigated, but the FET method failed to detect any superharmonic response. On the other hand, the harmonic balance predicts an SHR2 that is found in close agreement with the observed experimental results. In a second attempt to obtain the SHR2, the same problem was treated, but an extremely small initial imperfection was added to the beam. The initial imperfection consists of a sine-wave lateral deflection with a maximum midspan deflection of 1/500 the thickness of the beam (i.e., 2.5×10^{-06} its length). Figure 5 shows the experimental results for the SHR2, which agree closely with the prediction of the HB method and the FET results for the beam with an initial imperfection. Note that the initial imperfection modifies the first natural frequency of the beam, but this has no effect on the nondimensional plot.

The previous example calls for further discussion: why did the FET approach fail to detect the SHR2 of a straight beam? An important element in this discussion comes from another analytical approach to the problem: the multiple time scales (MTS) method,[10] which was used to solve in detail the problem at hand in Refs. 19 and 20. The MTS method predicts that a system with cubic nonlinearities will exhibit resonances not only for $\bar{\omega} = 1/3$ or 3/1 but also for $\bar{\omega} = n/m$ (n and m are integers), like $\bar{\omega} = 1/2$ and 3/2, etc., at the higher perturbation levels. The initially straight beam possesses cubic nonlinearities only, whereas an initial imperfection introduces additional quadratically nonlinear terms in the problem. Hence, an analytical solution of the problem with the MTS method predicts SHR2 as a primary resonance only for beams with an initial imperfection, but as higher-order resonance for straight beams.[19,20] This means that the SHR2 of a straight beam occurs over an extremely narrow frequency range (much narrower than the primary resonance at $\bar{\omega} = 1/3$), and it is hence possible that the FET analysis was conducted outside that narrow range, failing to detect the resonance. It is important to note that extremely small initial imperfections (2.5×10^{-06} times the length of the beam) are sufficient for the system to exhibit the SHR2 as a primary resonance.

It is most likely that the physical system used in the experiment did indeed present such a small initial imperfection, and this suggests that the experimentally observed SHR2 might be a result from this initial imperfection. The confusing fact in this discussion is that the analytical prediction of the SHR2 amplitude of a straight beam using the HB method closely agrees with the FET predictions for a beam with an initial imperfection. On the other hand, if the excitation function is $\sin\omega_f t$, the HB prediction of the SHR2 of a straight beam is $\sin 2\omega_f t$, whereas the FET prediction of the SHR2 of an imperfect beam is $\cos 2\omega_f t$ (in agreement with the HR solution of an imperfect beam[21]). Experimental phase information unfortunately was not reported in Ref. 18, but such measurement would provide a more definite conclusion about this problem.

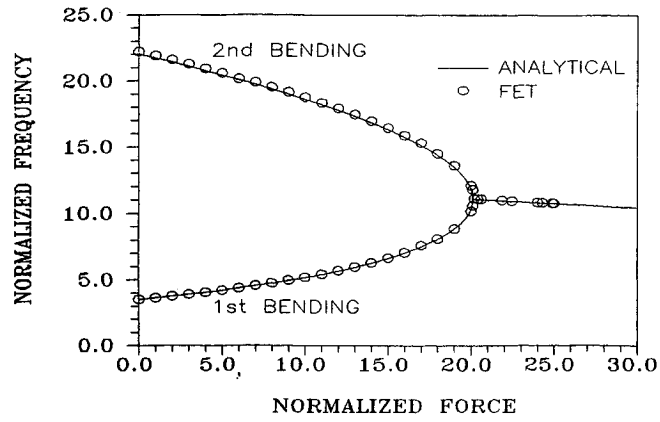

a) Two lowest bending frequencies of the beam vs the normalized follower force λ

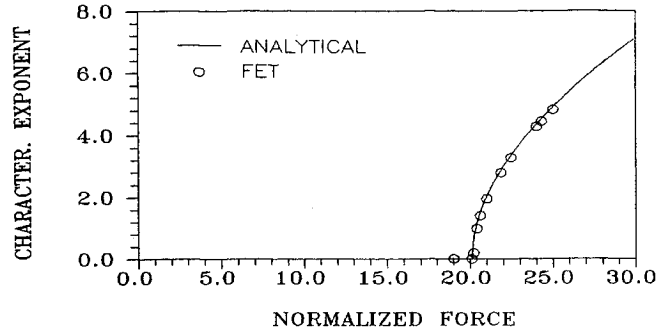

b) Characteristic exponent of the system vs the normalized follower force λ

Fig. 6 Linearized stability analysis of a cantilevered beam under a tip follower force.

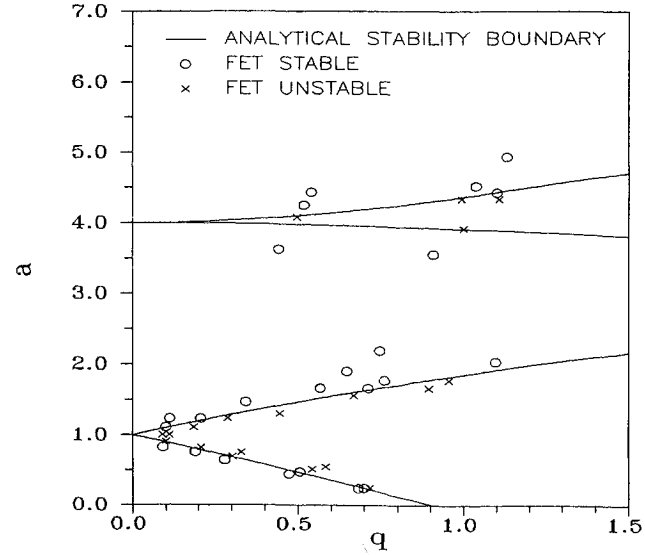

Fig. 7 Stability boundaries for a parametrically excited clamped-clamped beam.

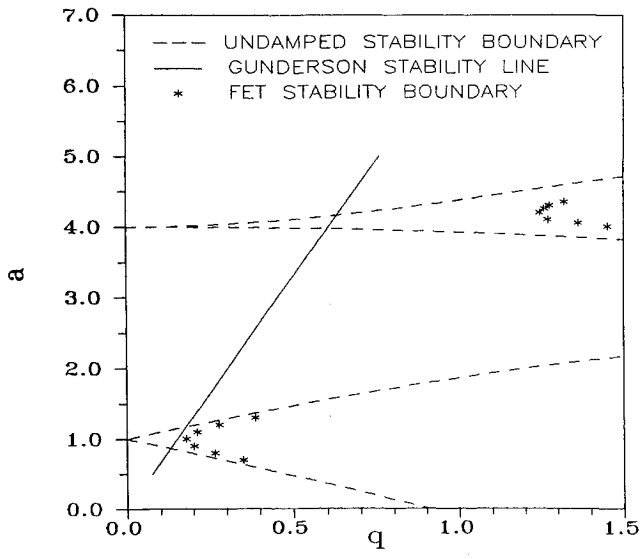

Fig. 8 Stability boundaries for a parametrically excited clamped-clamped beam with viscous damping forces ($\zeta = 0.1$).

The third example is a stability analysis of a beam subjected to a tip compressive follower force of magnitude P. The properties of the beam are the same as in the previous example. Two cubic elements were used to model the beam and 32 time nodes (eight quartic elements) to model one period. Solutions of this classical problem exist; see, for instance, Bolotin[22] for an exact solution and Bailey and Haines[23] for a numerical solution. Since the excitation does not vary in time, any period could be used for the FET model of this problem, and in this example the period of the lowest bending mode of the unloaded beam was selected.

A linearized stability analysis based on the eigenvalues of the transfer matrix was performed for various magnitudes of the follower force. Figure 6a shows the two lowest bending frequencies of the system vs the nondimensionalized follower force amplitude $\lambda = PL^2/EI$. The analytical solution[22] closely agrees with the FET predictions. Instability occurs at the frequency coalescence point, where one of the eigenvalues of the transfer matrix becomes larger than unity, expressing an exponentially growing solution. Figure 6 shows this characteristic exponent as predicted by the analytical solution and the FET approach. Good correlation is found.

The last example is another classical problem: the parametric excitation of a beam under a pulsating axial load. The beam is clamped at one end, and at the other end the axial displacement is free, but all other displacement components are constrained. This problem was treated extensively in the literature.[24-27] The properties of the beam are the same as in the previous example. Two elements were used to model the span of the beam and 32 time nodes (eight quartic elements) to model one period. At first, no damping forces were applied. Figure 7 shows a summary of the stability analysis on a q vs a plot, where

$$a = 4\,(\omega_1/\Omega)^2 \tag{45a}$$

$$q = \tfrac{1}{2} a (P/P_{cr}) \tag{45b}$$

where Ω is the excitation frequency, ω_1 the first natural bending frequency, P the magnitude of the pulsating force, and P_{cr} the critical Euler buckling load of the beam. The solid curves are the analytical predictions of the stability boundaries based on a modal approximation followed by a perturbation solution of the resulting Mathieu equation.[27] Two instability regions were investigated, around $a = 1$ and 4, respectively. The symbols indicate the FET results, and the stability boundaries are found in close agreement for both regions.

Finally, the effect of viscous damping forces on the behavior of the beam was analyzed. The effect of damping is to shrink the instability regions. The exact shape of the instability boundaries in the presence of damping is rather difficult to obtain analytically; however, approximate stability conditions are available.[27,28] Figure 8 shows analytical predictions of the stability boundary without damping, the approximate prediction in the presence of damping, and the FET results. The damping parameter was $\zeta = 0.1$, where $\zeta = \mu/m\Omega$.

VIII. Conclusions

A formulation of nonlinear periodic beam problems based on the finite element in time approach was presented in this paper. This method allows the prediction of the periodic response of mechanical systems as well as linearized stability analysis about that periodic solution with the help of Floquet's theory. There are several advantages to the FET approach:

1) Periodic boundary conditions are readily imposed on nonlinear systems.

2) The same solution procedure can be applied for both the periodic solution calculation and stability analysis, which requires the knowledge of the transfer matrix, a byproduct of the periodic solution calculations.

3) The versatility of the finite-element procedure allows the treatment of complex problems in space, and the finite element in time discretization naturally results in higher-order, efficient time integration procedures.

4) The predictions of the FET method for several classical nonlinear dynamic problems were found in good agreement with the analytical solutions and experimental results when available.

In summary, the finite element in time approach appears ideally suited for the analysis of both periodic response and linearized stability boundaries of nonlinear periodic systems.

Appendix A

The nonzero components of the mass matrix I defined in Eq. (17) are

$$I_{11} = I_{22} = I_{33} = m,\ I_{44} = m_{11},\ I_{55} = m_{22},\ I_{66} = m_{33}$$

$$I_{15} = m_3,\ I_{16} = -m_2,\ I_{24} = -m_3,\ I_{34} = m_2,\ I_{56} = -m_{23}$$

where the various mass coefficients are defined as

$$m = \int_\Gamma \rho\, ds,\ m_2 = \int_\Gamma \rho x_2 ds,\ m_3 = \int_\Gamma \rho x_3\, ds$$

$$m_{22} = \int_\Gamma \rho x_2^2\, ds,\ m_{33} = \int_\Gamma \rho x_3^2\, ds,\ m_{23} = \int_\Gamma \rho x_2 x_3\, ds$$

$$m_{11} = m_{22} + m_{33}$$

Appendix B

The nonvanishing components of the $\tilde{D}_n$ matrix are

$$\tilde{D}_{11} = -\mu_1,\quad \tilde{D}_{22} = -\mu_2,\quad \tilde{D}_{33} = -\mu_3,$$

$$\tilde{D}_{44} = -\mu_\alpha,\quad \tilde{D}_{55} = -\mu_\beta,\quad \tilde{D}_{66} = -\mu_\gamma$$

The nonvanishing components of the D_n matrix are

$$D_{14} = -F_f S\alpha C\beta$$

$$D_{15} = -F_f C\alpha S\beta$$

$$D_{25} = -F_f C\beta$$

$$D_{34} = F_f C\alpha C\beta$$

$$D_{35} = -F_f S\alpha S\beta$$

Acknowledgments

This research was sponsored by the Army Research Office under Grant DAAG 29-82-K-0093, with Dr. Robert Singleton as contract monitor.

References

[1]Houbolt, J. C., "A Recurrence Matrix Solution for the Dynamic Response of Elastic Aircraft," *Journal of Aeronautical Sciences,* Vol. 17, March 1950, pp. 540–550.

[2]Newmark, N. M., "A Method of Computation for Structural Dynamics," *ASCE Journal of the Engineering Mechanics Division,* Vol. 85, 1959, pp. 67–94.

[3]Wilson, E. L., Farhoomand, I., and Bathe, K.J., "Nonlinear Dynamic Analysis of Complex Structures," *International Journal of Earthquake Engineering and Structural Dynamics,* Vol. 1, Feb. 1973, pp. 241–252.

[4]Bailey, C. D., "Application of Hamilton's Law of Varying Action," *AIAA Journal,* Vol. 13, Sept. 1975, pp. 1154–1157.

[5]Leipholtz, H. H. E., "Space-Time Formulation of Hamilton's Law," *Mechanics Research Communications,* Vol. 9, May 1982, pp. 317–323.

[6]Borri, M., Ghiringhelli, L., Lantz, M., Mantegazza, P., and Merlini, T., "Dynamic Response of Mechanical Systems by a Weak Hamiltonian Formulation," Symposium on Advances and Trends in Structures and Dynamics, Arlington, VA, Oct. 1984.

[7]Serbin, S. M., "On a Fourth-Order Unconditionally Stable Scheme for Damped Second-Order Systems," *Computer Methods in Applied Mechanics and Engineering,* Vol. 23, March 1980, pp. 333–340.

[8]Dougalis, V. A. and Serbin, S. M., "On Some Unconditionally Stable, Higher Order Methods for the Numerical Solution of the Structural Dynamics Equations," *International Journal for Numerical Method in Engineering,* Vol. 18, Nov. 1982, pp. 1613–1621.

[9]Felippa, C. A. and Park, K. C., "Computational Aspects of Time Integration Procedures in Structural Dynamics; Part 1: Implementation; Part 2: Error Propagation," *Journal of Applied Mechanics,* Vol. 45, Sept. 1978, pp. 595–602 and 603–611.

[10]Nayfeh, A. H. and Mook D. T., *Nonlinear Oscillations,* Wiley-Interscience, New York, 1979, pp. 161–200.

[11]Bauchau, O. A. and Hong, C. H., "Nonlinear Composite Beam Theory," *Journal of Applied Mechanics,* Vol. 110, March 1988, pp. 156–163.

[12]Bauchau, O. A. and Hong, C. H., "Large Displacement Analysis of Naturally Curved and Twisted Beams," *AIAA Journal,* Vol. 25, Nov. 1987, pp. 1469–1475.

[13]Washizu, K., *Variational Methods in Elasticity and Plasticity,* Pergamon, New York, 1975, pp. 76–92.

[14]Wempner, G., *Mechanics of Solids with Application to Thin Bodies,* Sijthoff and Noordhoff, 1981.

[15]Bellmann, R. E. and Kalaba, R. E., *Quasilinearization and Nonlinear Boundary Value Problems,* American Elsevier, New York, 1965, pp. 135–173.

[16]Bathe, K. J., *Finite Element Procedures in Engineering Analysis,* Perentice-Hall, Englewood Cliffs, NJ, 1982, pp. 194–249.

[17]Hodges, D. H. and Rutkowski, M. J., "Free Vibration Analysis of Rotating Beams by a Variable-Order Finite Element Method," *AIAA Journal,* Vol. 19, Nov. 1981, pp. 1459–1466.

[18]Tseng, W. Y. and Dugundji, J., "Nonlinear Vibrations of a Beam Under Harmonic Excitation," *Journal of Applied Mechanics,* Vol. 37, June 1970, pp. 292–297.

[19]Bennett, J. A. and Rinkel, R. L., "Ultraharmonic Vibrations of Nonlinear Beams," *AIAA Journal,* Vol. 10, May 1972, pp. 715–716.

[20]Bennett, J. A., "Ultraharmonic Motion of a Viscously Damped Nonlinear Beam," *AIAA Journal,* Vol. 11, May 1973, pp. 710–715.

[21]Tseng, W. Y. and Dugundji, J., "Nonlinear Vibrations of a Buckled Beam under Harmonic Excitation," *Journal of Applied Mechanics,* Vol. 38, June 1971, pp. 467–476.

[22]Bolotin, V. V., *Non Conservative Problems of the Theory of Elastic Stability,* Pergamon Press, New York, 1963, pp. 86–134.

[23]Bailey, C. D. and Haines, J. L., "Vibration and Stability of Non-Conservative Follower Force Systems," *Computer Methods in Applied Mechanics and Engineering,* Vol. 26, Jan. 1981, pp. 1–31.

[24]Hsu, C.S., "On the Parametric Excitation of a System Having Multiple Degrees of Freedom," *Journal of Applied Mechanics,* Vol. 30, No. 1, March 1963, pp. 367–372.

[25]Iwatsubo, T. and Saigo, M., "Parametric Instability of Clamped-Clamped and Clamped-Simply Supported Columns under Periodic Axial Load," *Journal of Sound and Vibration,* Vol. 30, Jan. 1973, pp. 65–77.

[26]Friedmann, P.P., Hammond, C.E., and Woo, T. H., "Efficient Numerical Treatment of Periodic Systems with Application to Stability Problems," *International Journal of Numerical Methods in Engineering,* Vol. 11, No. 9, 1977, pp. 1117–1136.

[27]Richard, J. A., *Analysis of Periodically Time-Varying Systems,* Springer-Verlag, New York, 1983, pp. 123–151.

[28]Gunderson, H., Rigas, H., and van Vleck, F.S., "A Technique for Determining Stability Regions for the Damped Mathieu Equation," *SIAM Journal of Applied Mathematics,* Vol. 26, 1974, pp. 345–349.